Article

Cell Reports

From Hyper- to Hypoinsulinemia and Diabetes: Effect of KCNH6 on Insulin Secretion

Graphical Abstract

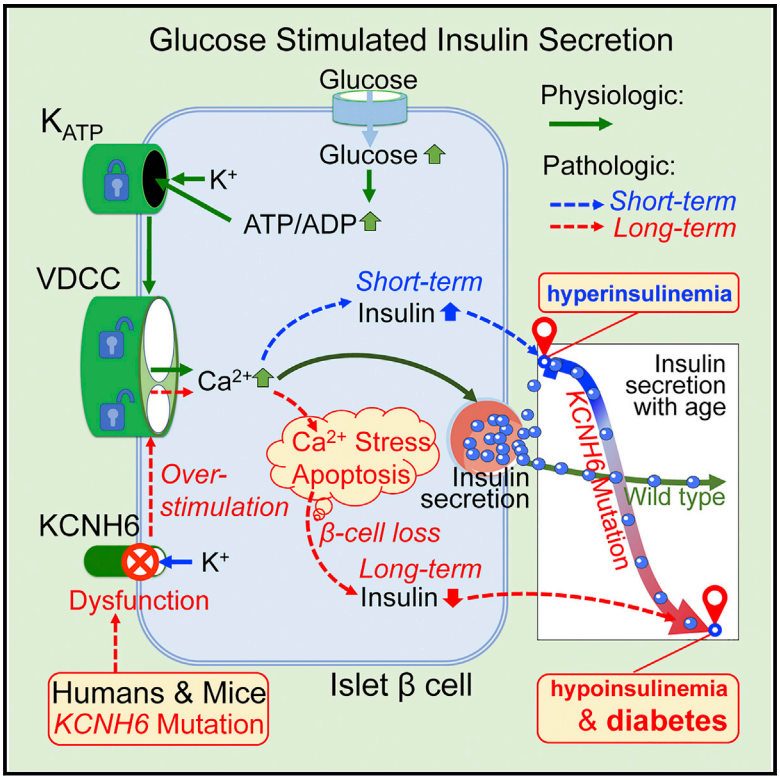

Highlights

- KCNH6 regulates insulin secretion and glucose hemostasis in humans and mice
- KCNH6 dysfunction causes a phenotype from hyper- to hypoinsulinemia and diabetes
- KCNH6 dysfunction increases intracellular calcium levels and hyperinsulinemia
- Chronic elevation of intracellular calcium causes β cell loss and hypoinsulinemia

Authors

Jin-Kui Yang, Jing Lu, Sha-Sha Yuan, ..., George Liu, Xiu-Qing Zhang, Aimin Xu

Correspondence

jkyang@ccmu.edu.cn

In Brief

Yang et al. show that KCNH6 plays a key role in insulin secretion and glucose hemostasis in humans and mice. Dysfunction of KCNH6 results in a hyperinsulinemia phenotype in the short term and hypoinsulinemia and diabetes in the long term.

Yang et al., 2018, Cell Reports *25*, 3800–3810
December 26, 2018
https://doi.org/10.1016/j.celrep.2018.12.005

CellPress

OPEN ACCESS
CellPress

Cell Reports
Article

From Hyper- to Hypoinsulinemia and Diabetes: Effect of KCNH6 on Insulin Secretion

Jin-Kui Yang,[1,12,13,*] Jing Lu,[1,12] Sha-Sha Yuan,[1,12] Asan,[2,12] Xi Cao,[1] Hai-Yan Qiu,[1] Ting-Ting Shi,[1] Fang-Yuan Yang,[1] Qian Li,[1] Cui-Ping Liu,[4] Qian Wu,[5] Yu-Hui Wang,[6] Hai-Xia Huang,[7] Abudurexiti Kayoumu,[6] Jian-Ping Feng,[1] Rong-Rong Xie,[1] Xiao-Rong Zhu,[1] Chang Liu,[1] Guang-Ran Yang,[1] Ming-Rong Zhang,[9] Chun-Lan Xie,[9] Chen Chen,[8] Bo Zhang,[5] George Liu,[6] Xiu-Qing Zhang,[3,9] and Aimin Xu[10,11]

[1]Beijing Key Laboratory of Diabetes Research and Care, Beijing Tongren Hospital, Capital Medical University, Beijing 100730, China
[2]Binhai Genomics Institute & Tianjin Translational Genomics Center, BGI-Tianjin, BGI-Shenzhen, Tianjin 300308, China
[3]Guangzhou Key Laboratory of Cancer Trans-Omics Research, BGI-Guangzhou, BGI-Shenzhen, Guangzhou 510006, China
[4]Department of Endocrinology, Beijing Chuiyangliu Hospital, Beijing 100022, China
[5]Key Laboratory of Cell Proliferation and Differentiation of the Ministry of Education, College of Life Sciences, Peking University, Beijing 100871, China
[6]Key Laboratory of Molecular Cardiovascular Science of the Ministry of Education, Institute of Cardiovascular Science, Peking University, Beijing 100083, China
[7]Department of Physiology and Pathophysiology, School of Basic Medical Sciences, Capital Medical University, Beijing 100069, China
[8]School of Biomedical Sciences, University of Queensland, Brisbane 4072, Australia
[9]The Guangdong Enterprise Key Laboratory of Human Disease Genomics, BGI-Shenzhen, Shenzhen 518083, China
[10]State Key Laboratory of Pharmaceutical Biotechnology, University of Hong Kong, Pokfulam, Hong Kong
[11]Department of Medicine, University of Hong Kong, Pokfulam, Hong Kong
[12]These authors contributed equally
[13]Lead Contact
*Correspondence: jkyang@ccmu.edu.cn
https://doi.org/10.1016/j.celrep.2018.12.005

SUMMARY

Glucose-stimulated insulin secretion from islet β cells is mediated by K_{ATP} channels. However, the role of non-K_{ATP} K^+ channels in insulin secretion is largely unknown. Here, we show that a non-K_{ATP} K^+ channel, KCNH6, plays a key role in insulin secretion and glucose hemostasis in humans and mice. KCNH6 p.P235L heterozygous mutation co-separated with diabetes in a four-generation pedigree. *Kcnh6* knockout (KO) or *Kcnh6* p.P235L knockin (KI) mice had a phenotype characterized by changing from hypoglycemia with hyperinsulinemia to hyperglycemia with insulin deficiency. Islets from the young KO mice had increased intracellular calcium concentration and increased insulin secretion. However, islets from the adult KO mice not only had increased intracellular calcium levels but also had remarkable ER stress and apoptosis, associated with loss of β cell mass and decreased insulin secretion. Therefore, dysfunction of KCNH6 causes overstimulation of insulin secretion in the short term and β cell failure in the long term.

INTRODUCTION

Glucose-stimulated insulin secretion (GSIS) from pancreatic islet β cells is regulated by a series of electrogenic events. This electrogenic mechanism is generally referred to as the ATP-sensitive potassium (K_{ATP}) channel pathway. Metabolism of glucose leads to an increase in the ATP/ADP ratio. This increase causes closure of K_{ATP} channels, depolarization of the plasma membrane, influx of calcium through voltage-gated calcium channels (VDCCs), and exocytosis of insulin secretory granules. However, during depolarization-induced action potentials, other K^+ channels may responsible for action potential duration and frequency, as well as for the repolarization of β cells (Braun et al., 2008; Houamed et al., 2010).

Studies *in vitro* have shown evidence for non-K_{ATP} channel stimulation of insulin secretion by glucose, especially a role for voltage-dependent K^+ (Kv) channels as modulators of insulin secretion (Félix-Martínez and Godínez-Fernández, 2014; Yang et al., 2014). Reports have also shown that the ether-a-go-go-related gene (ERG) channel is an active participant in the regulation of β cell electrical activity and insulin secretion in the rat pancreas and β cells *in vitro* (Mühlbauer et al., 2007). Glucose-dependent stimulation of insulin secretion from Kv channel blockers has been reported in rodent islets and insulinoma cells (MacDonald et al., 2001, 2002).

ERG-class channels are members of a larger family of Kv channels. Three isoforms, KCNH2 (ERG), KCNH6 (ERG2), and KCNH7 (ERG3), have been discovered (Shi et al., 1997). Long QT syndrome, a dominant inherited channelopathy that can result in sudden cardiac death, is caused by human KCNH2 (Kv11.1) heterozygous mutations (Sanguinetti et al., 1995). A report indicates that patients with long QT syndrome due to loss-of-function mutation of KCNH6 have reactive high insulin secretion associated with reactive hypoglycemia after an oral glucose tolerance test (OGTT) (Hyltén-Cavallius et al., 2017).

It was reported that 3% of hyperglycemic adults diagnosed as having type 2 diabetes (T2D) are affected by a multigenerational

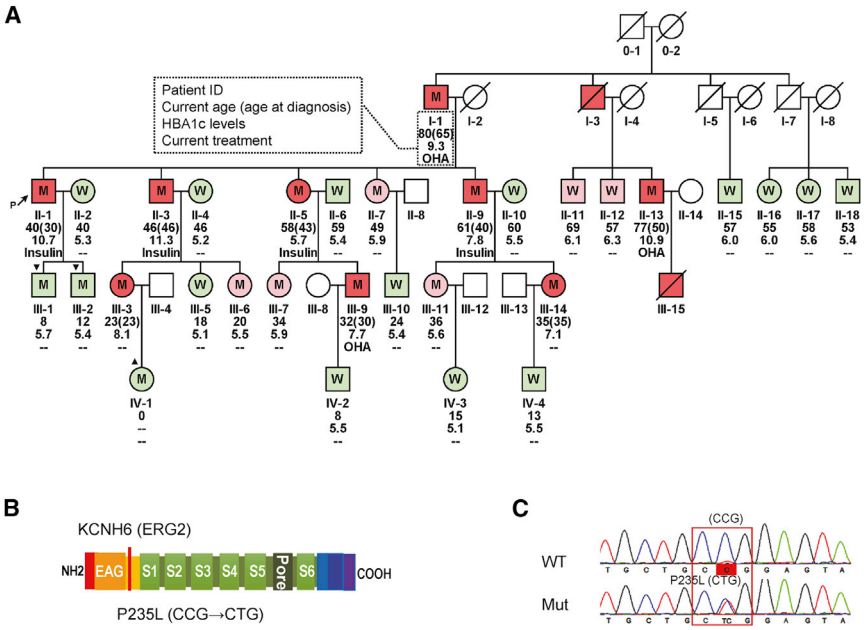

Figure 1. *KCNH6* Mutations in a Four-Generation Pedigree with Multigenerational Monogenic Diabetes

(A) Four-generation diabetes pedigree with *KCNH6* gene mutations. The proband is marked by an arrow. Females are represented by circles, and males are represented by squares. Subjects marked with green, pink, and red are normal glucose tolerance (NGT), impaired glucose tolerance (IGT), and diabetes mellitus (DM), respectively. Patient ID, current age (age of diagnosis), HbA1c levels, and current treatment are listed below the circles or squares. ▼, childhood *KCNH6* mutant subjects with hyperinsulinemia; ▲, a newborn *KCNH6* mutant baby with severe neonatal hypoglycemia; OHA, oral hypoglycemic agents; M, heterozygous *KCNH6* p.P235L mutation; W, wild-type; ►, prediabetes defined by an oral glucose tolerance test (OGTT).

(B and C) Family with monogenic diabetes had KCNH6 heterozygous p.P235L mutations (P235L). (B) Cartoon of one of the four subunits of KCNH6 channels. The N-terminal Per-Arnt-Sim (PAS) domain preceded by a conserved sequence of 25–27 amino acids (PAS-cap) is in red. The ether-a-go-go (EAG) is in orange. The C-linkers, the C-terminal cyclic nucleotide binding homology domain (CNBHD), and post-CNBHD domains are in aquamarine, blue, and purple, respectively.

(C) DNA sequences of the *KCNH6* wild-type (WT) phenotype and P235L mutation.

disease (Ludovico et al., 2015; Pezzilli et al., 2018). Here we first show the evidence from patients with multigenerational diabetes and two mouse models supporting the pivotal role of both human KCNH6 (Kv11.3) and mouse Kcnh6 in the regulation of insulin secretion. We linked *KCNH6* gene p.P235L mutation with diabetes in the pedigree. *KCNH6* knockout (KO) and p.P235L knockin (KI) mouse models mimicked the phenotype changing from hyperinsulinemia to hypoinsulinemia and diabetes found in the pedigree. This result suggests that KCNH6 plays a key role in insulin secretion and glucose hemostasis in humans and mice.

RESULTS

KCNH6 Mutation in a Four-Generation Pedigree

We have previously conducted a three-step programmed method for the identification of yet-unknown gene mutations of maturity-onset diabetes of the young (MODY-x) (Li et al., 2016). In 2009, we identified a four-generation family with multigenerational monogenic diabetes (Ludovico et al., 2015; Pezzilli et al., 2018) from a mountain village in central China (Figure 1A). We excluded mutations in all known high-frequency MODY-1, MODY-2, and MODY-3 genes (Horikawa et al., 1997; Vionnet et al., 1992; Yamagata et al., 1996a, 1996b) and K_{ATP}-related MODY genes, including *ABCC8* (MODY-12) (Bowman et al., 2012) and *KCNJ11* (MODY-13) (Bonnefond et al., 2012), in the proband.

In 2010, we performed whole-exome sequencing on four affected individuals (II-1, III-3, III-9, and III-14) who were diagnosed with diabetes at 30, 23, 30, and 35 years of age, respectively (Figure 1A; Tables S1 and S2). After filtering (Table S3) and being validated in all family members by Sanger sequencing, only the heterozygous p.P235L mutation (Mut) in the *KCNH6* gene (GenBank: NM_030779.2; c.704T > C) (Figure 1B) co-separated with the diabetic phenotype. Biochemical parameters were the same except that the Mut group had higher plasma glucose, uric acid, and low-density lipoprotein (LDL) cholesterol levels (Table S4).

KCNH6 Muts in Other Patients with Multigenerational Diabetes

We sequenced the gene in a panel of 99 patients with early-onset multigenerational diabetes (Thanabalasingham and Owen, 2011). We identified two families with heterozygous missense Mut (p.R385G and p.R715W) that were not reported in the public database dbSNP v.135 (Figures S1A–S1C; Table S5). *KCNH6* p.P235L, p.R385G, and p.R715W muts were predicted to be probably damaging protein function by PolyPhen2, with scores of 0.990, 0.971, and 0.999, respectively (Figure S1D). Furthermore, these three Muts were predicted to be causing disease by MutationTaster. This implies that *KCNH6* Mut may not be a rare finding in Chinese patients with early-onset multigenerational diabetes.

From Hyper- to Hypoinsulinemia and Diabetes

In 2014, a baby (IV-1) with neonatal hypoglycemia was born to patient III-3. This baby had blood glucose levels of 1.3 and 2.2 mmol/L before and after glucose treatment, respectively.

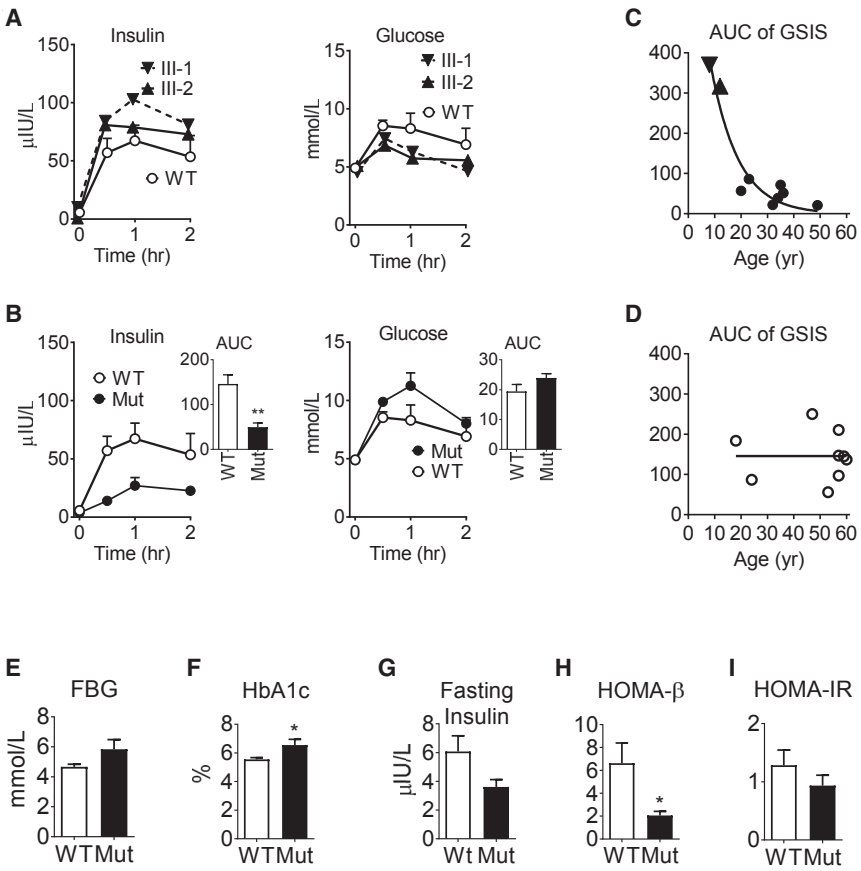

Figure 2. Clinical Parameters of the Family Members

(A) Elevated glucose-stimulated insulin secretion (left) and relatively low blood glucose levels (right) during an oral glucose tolerance test (OGTT) in childhood mutant family members.

(B) Decreased insulin secretion during OGTT for adulthood mutant family members.

(C) Reduced area under the curve (AUC) of insulin secretion with age for mutant family members.

(D) AUC of insulin secretion for WT family members.

(E) Fasting blood glucose (FBG).

(F) Hemoglobin A1c (HbA1c).

(G) Fasting insulin (F-Ins).

(H) The Homeostasis Model Assessment (HOMA) index of β cell function (HOMA-β).

(I) HOMA index of insulin resistance (HOMA-IR).

▼, childhood *KCNH6* mutant subjects with hyperinsulinemia; ●, mutant adults without previously diagnosed diabetes (n = 7); ○, WT adults (n = 9). Values represent means ± SEM. *p < 0.05 versus WT. Significance values were calculated using the Mann-Whitney U test.

The newborn with neonatal hypoglycemia is a P235L genotype of *KCNH6*, although no informed consent was obtained for further blood tests. Furthermore, high blood insulin levels and relatively low blood glucose levels were found in two P235L children in the pedigree (Figure 2A). *KCNH6* p.V532F heterozygous Mut was previously reported to be a suspected cause of neonatal hypoglycemia with hyperinsulinemia in an Italian family (Proverbio et al., 2013).

In contrast, hypoinsulinemia was found in adult P235L family members (Figure 2B). Insulin secretion decreased with age for the P235L patients (Figure 2C), but not for wild-type phenotype (WT) family members (Figure 2D). Of the 13 adult Mut members, all had glucose intolerance (6 with previously diagnosed diabetes, 3 with newly diagnosed diabetes, and 4 with impaired glucose tolerance [IGT]). The P235L patients had higher glucose levels (Figure 2E) and hemoglobin A1c (HbA1c) levels (Figure 2F) and lower islet β cell function (Figures 2G–2I). However, of the WT adult members, 2 had IGT and none had diabetes. Therefore, we speculate that *KCNH6* p.P235L Mut causes monogenic diabetes characterized by childhood hyperinsulinemia and adulthood hypoinsulinemia and diabetes.

Characteristics and Expression Profiles of KCNH2

Loss-of-function Mut of the *KCNH2* gene can cause long QT syndrome (Hyltén-Cavallius et al., 2017). In this pedigree, none of those with *KCNH6* Mut suffered from the syndrome when tested by electrocardiogram (Figure S2), although an obvious long QT interval is not always seen for patients with this syndrome.

The protein sequence around the P235L Mut is highly conserved not only in the orthologs of the *KCNH62* gene across species, including rhesus, mouse, dog, chicken, and zebrafish (Figure S1E), but also in the KCNH2-class family (*KCNH2*, *KCNH6*, and *KCNH7*) (Figure S1F). The significant conservation of this position suggests that the protein sequence including this Mut might play critical roles in protein function.

Previously, a study with single-cell transcriptomic analysis of human pancreatic islets indicated that KCNH6 mRNA was expression mainly in islet α cells (Segerstolpe et al., 2016). With real-time PCR assay, we found that KCNH6 was highly expressed in pancreas, heart, and kidney in humans, while KCNH2 was highly expressed in heart, lung, kidney, and pancreas in humans (Figure S3A). Double immunofluorescence staining with antibodies against KCNH6 and insulin demonstrated that KCNH6 protein was expressed in islet β cells in humans (Figure S3B) and mice (Figure S3C).

KCNH6 p.P235L Is a Dominant-Negative Mut

To examine the functional impact of *KCNH6* p.P235L Mut on the KCNH6 channels, a patch-clamp experiment was performed. We constructed plasmids encoding human (wild-type [WT]) and homozygous (m/m) *KCNH6* p.P235L mutant,

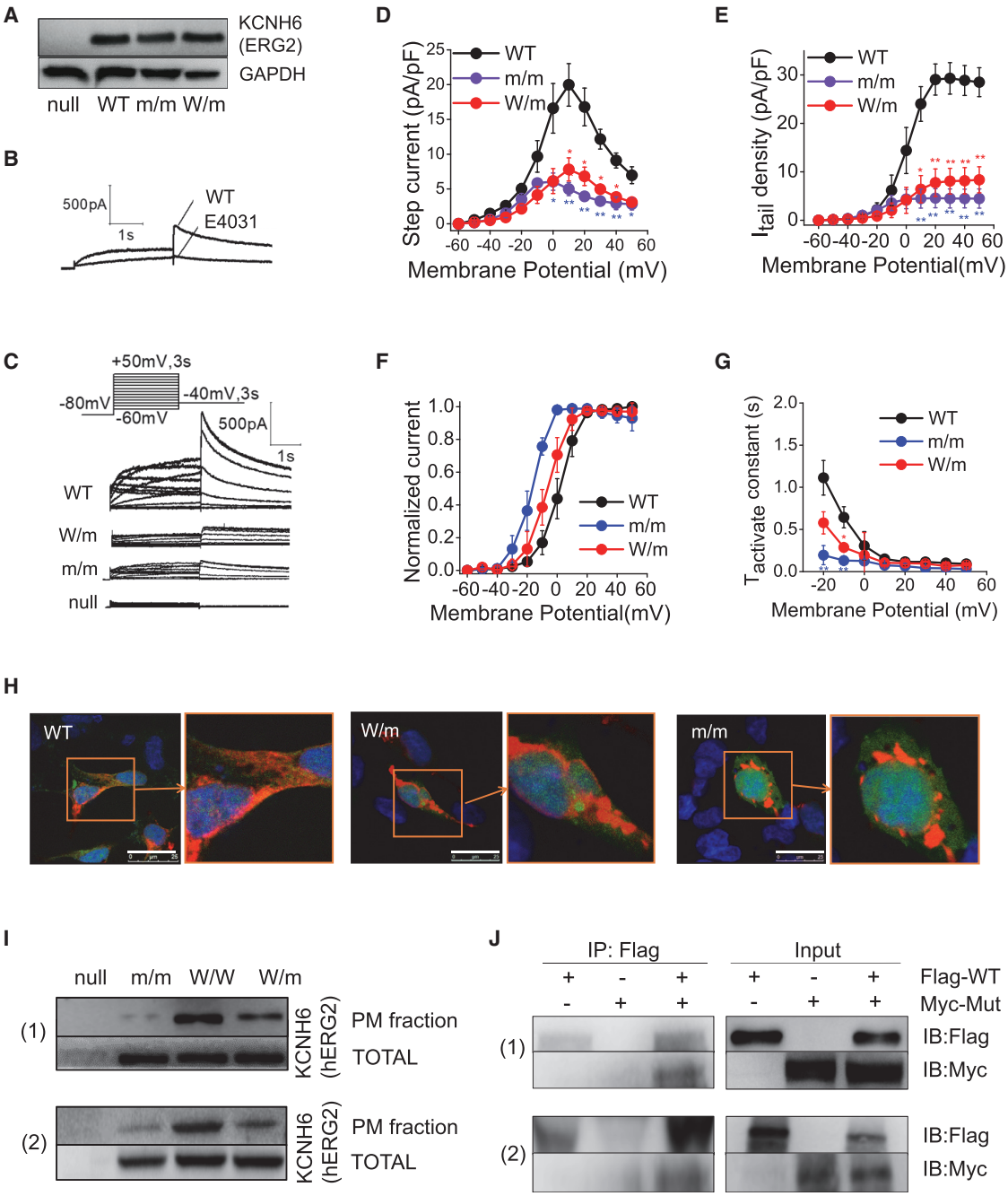

Figure 3. Electrophysiology and Immunohistochemistry Analysis of the p.P235L Mutant KCNH6 Channel

(A–G) Voltage-clamp records of KCNH6 channels in KCNH6 null HEK293 cells transiently transfected with plasmids encoding null, WT, homozygous (m/m), and heterozygous (W/m) mutant human KCNH6 (p.P235L).

(A) Representative western blot of KCNH6 protein.

(B) Representative KCNH6 current traces (50 mV) for HEK293 cells transfected with WT KCNH6 treated with E4031, a specific blocker of ERG channels.

(C) Representative current traces for HEK293 cells transfected with WT, W/m, m/m, and null KCNH6. The protocol of the depolarized voltage was from −60 to 50 mV for 3 s, and the repolarization voltage was −40 mV.

(D) Step current as measured from the triangles.

(E) Tail current as measured from the peak current.

(F) Normalized tail current as measured from the peak current that fitted with a Boltzmann function. Half-maximal activation (V1/2) and slope (k) factors for the activation and inactivation data were calculated using a Boltzmann function: $I = Imax/(1 + \exp[(V1/2 - X)/k])$ for activation, where X is the test membrane potential.

(G) Time constants (τ) for activation were calculated using a single exponential function: $Y = Y0 + A \times \exp[-(1/\tau) \times t]$, where Y0 is the baseline current, A is the amplitude of the exponential relaxation, and t is the time.

(legend continued on next page)

which was then transfected into KCNH6 null HEK293 cells. WT and m/m *KCNH6* were transfected at a 1:1 ratio into HEK293 cells as heterozygous (W/m). Similar levels of KCNH6 protein expression (Figure 3A) were detected in HEK293 cells transiently transfected with plasmids encoding the WT, m/m, and W/m *KCNH6*. E4031, a blocker of KCNH2 channels, was used as a channel-specific control (Figure 3B). Representative KCNH6 current traces for WT-, W/m-, and m/m-transfected and WT-, W/m-, and m/m-untransfected HEK293 cells recorded by patch clamp are shown (Figure 3C). Compared with WT, m/m and W/m had lower step-current density (Figure 3D) and tail-current density (Figure 3E). Other electrophysiological properties, including steady-state inactivation, deactivation curve, and recovery curve (Figure S4), were similar among the three groups. The steady-state activation curve (Figure 3F) and time constant of activation of the currents (Figure 3G) indicated that m/m and W/m had a quicker activation property than WT.

Current density indicates overall channel function. Although results of the gating kinetics indicated that *KCNH6* p.P235L is not a dysfunction Mut, overall function of the channel can be affected by two factors: the gating kinetics and the amount of channel on the plasma membrane or membrane targeting.

We then investigated membrane targeting and compared the subcellular localization of the WT and the P235L channel protein using immunocytochemistry and western blot analysis. The result indicated that while most WT KCNH6 was distributed at the plasma membrane, the m/m and W/m KCNH6 channels were clustered around the cell nucleus, rather than on the cell membrane (Figure 3H). Western blot analysis for subcellular fractions also showed that levels of m/m and W/m KCNH6 expressed in the cell membrane were significantly lower than those of WT KCNH6 in two independent studies (Figure 3I). Thus, the WT/P235L (W/m) Mut-induced dominant dysfunction of KCNH6 channels was attributed to impaired subcellular trafficking and localization of the protein to the plasma membrane. Immunoprecipitation assay revealed interactions between WT and m/m in two independent studies (Figure 3J). These results indicate that dominant dysfunction of W/m *KCNH6* p.P235L Mut may be caused by interactions between WT protein and p.P235L mutant protein, because KCNH6 channels are tetramers of four identical subunits arranged as a ring, with each ring contributing to the wall of the transmembrane K^+ pore (Haitin et al., 2013) (Figure S1A).

Knockdown of *Kcnh6* in INS-1 β Cells

Because *KCNH6* p.P235L is a dysfunctional Mut, we propose that downregulation of KCNH6 may influence insulin secretion. We used short hairpin RNA (shRNA) to knockdown the mRNA expression of *Kcnh6* in the rodent INS-1 β cells (Figure S5A). *Kcnh6* knockdown enhanced glucose-induced elevation of the intracellular calcium concentrations (Figure S5B). Consistently, *Kcnh6* knockdown significantly enhanced insulin secretion at a high glucose concentration (Figure S5C).

Diabetes in *Kcnh6* KO Mice

To test whether loss-of-function Mut of the KCNH6 channel influences glucose homeostasis and insulin secretion found in the family with *KCNH6* Mut, we used our previously reported TALEN-based method (Zu et al., 2013) to create *Kcnh6* gene KO mice (Figure 4A). A TALEN pair targeting exon 5 of the *Kcnh6* gene (around the p.P235L Mut) in C57BL/6 mice was designed. The binding sites of left and right TALENs are specific for target sequences in *Kcnh6* that are unique within the KCNH2-class genes (Figure S6). From western and immunohistochemistry experiments, KCNH6 was expressed in insulin-secreting islet β cells in both humans and mice (Figure 4B; Figure S4B). In neonatal KO mice, random plasma glucose levels were low while the corresponding plasma insulin levels had a high trend compared to age-matched WT controls (Figure 4C). However, in 14-week-old young-adult KO mice, fasting plasma glucose levels were high while the corresponding plasma insulin levels were low compared to age-matched WT controls (Figure 4D). At the same time, blood glucose levels on an intraperitoneal glucose tolerance test (IPGTT) were significantly higher (Figure 4E), whereas the first- and second-phase insulin secretory responses to glucose were reduced (Figure 4F). With consecutive observations, the KO mice also showed significantly higher blood glucose levels on IPGTT when compared with the WT mice (Figure 4G). Insulin sensitivity of peripheral tissues in the KO mice showed no obvious difference compared with the WT mice at the age of 3 and 30 weeks, as evidenced by the insulin tolerance test (ITT) (Figure 4H). The weight and food intake of the KO mice had no significant change compared to WT (Figures S7A–S7C). GLP-1 and glucagon secretion were also unchanged at the age of 3 and 30 weeks (Figures S7D–S7G). Thus, *Kcnh6* KO mice had a phenotype characterized by changing from hyperinsulinemia to hypoinsulinemia and diabetes.

Diabetes in *Kcnh6* p.P235L KI Mice

We used a Cas9-based method targeting P235L of the C57BL/6N mouse *Kcnh6* gene to create *Kcnh6* p.P235L KI mice (Figures 5A and 5B; Figure S8). In neonatal KI mice, random plasma glucose levels were low while the corresponding plasma insulin levels were relatively high compared to age-matched WT controls (Figure 5C). Blood glucose levels on IPGTT were low at the age of 3 weeks (Figure 5D). In adult KI mice, blood glucose

(H) Immunofluorescence staining for localization of WT, W/m, and m/m KCNH6 channels expressed in HEK293 cells. Nuclei were counterstained with DAPI, which appears blue. KCNH6 is in red, and GFP is in green. All scale bars in white are 25 μm in length.

(I) Western blot analysis for KCNH6 protein from the total or from the plasma membrane (PM) fraction of HEK293 cells transfected with null, WT, W/m, and m/m human KCNH6.

(J) HEK293 cells transfected with plasmids encoding FLAG-WT, Myc-Mut, and FLAG-WT/Myc-Mut human KCNH6 was immunoprecipitated using an anti-FLAG affinity gel and immunoblotted with anti-FLAG (top panel) or anti-Myc antibodies (bottom panel).

Values represent means ± SEM. *$p < 0.01$, **$p < 0.001$ versus WT. Significance values were calculated using the Mann-Whitney U test ($n = 6$, 4, and 8 for WT, W/m, and m/m, respectively).

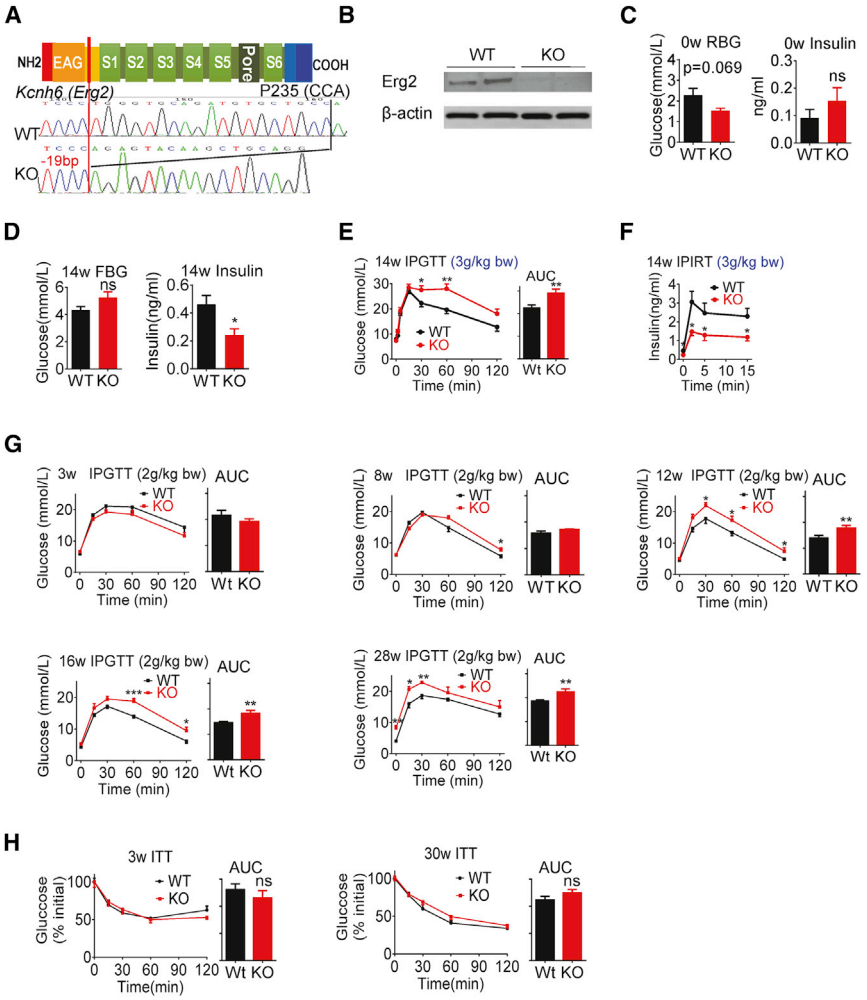

Figure 4. Mice with TALEN-Mediated Kcnh6 KO Mimic the Glucose Homeostasis of the Pedigree

(A and B) TALEN-mediated Kcnh6 knockout (KO) mice.

(A) Genotypes and DNA sequences of WT and −19 bp deletion frameshift KO.

(B) Western blot analysis of Kcnh6 protein in KO and WT mouse islets.

(C) Random blood glucose (RBG) (WT, n = 8; KO, n = 16) and plasma insulin (WT, n = 3; KO, n = 7) in neonatal mice.

(D) Fasting blood glucose and insulin levels at week 14 (WT, n = 9; KO, n = 11).

(E) Blood glucose levels and area under the curve (AUC) during an intraperitoneal glucose tolerance test (IPGTT) (3 g glucose/kg body weight [bw]) at week 14 (WT, n = 9; KO, n = 11).

(F) First- and second-phase insulin secretory responses to glucose IPGTT (3 g glucose/kg bw) at week 14 (WT, n = 9; KO, n = 11).

(G) Consecutive plasma glucose levels and area under the curve (AUC) during IPGTT (2 g glucose/kg bw) at weeks 3, 8, 12, 16, and 28 (WT, n = 7; KO, n = 7).

(H) Consecutive plasma glucose levels and area under the curve (AUC) during ITT (2 g glucose/kg bw) at weeks 3 and 30 (WT, n = 7; KO, n = 7).

Values represent means ± SEM. *$p < 0.05$, **$p < 0.01$, ***$p < 0.001$ versus WT. Significance values were calculated using Student's unpaired t test or the Mann-Whitney U test if $n < 9$.

levels on IPGTT were high (Figures 5E and 5G), while fasting insulin levels and the first- and second-phase insulin secretory responses to glucose (Figure 5F) were reduced. The weight and food intake of the KI mice were similar to those of the age-matched WT mice (Figure S9). Insulin sensitivity of peripheral tissues in the KI mice showed no obvious difference in comparing with the WT mice at the age of 3 and 30 weeks, as evidenced by the ITT (Figure 5H).

Kv Current and Action Potential of Mouse Pancreatic β Cells

We performed the electrophysiological experiment on the primary β cell from the KCNH6 KO and P235L KI mouse models. The amplitude of action potential is approximately 30–40 mV in magnitude from −55 mV, caused by high glucose stimulation in mouse β cells. In patch clamping, the amplitude of action potential is positively correlated with the injecting current stimulus (Guo et al., 2014). The Kv current of β cells from the KO and KI mice significantly decreased compared with that of the WT mice (Figures 6A and 6B). The magnitude of action potential was unaltered in the KO and KI and WT β cells. However, the duration of action potential, especially the repolarization time, was prolonged in the KO and KI β cells (Figures 6C–6E). These results indicate that the reduction of the Kv current in the KO and KI β cells may lead to the extension of action potential duration, which in turn can lead to an increase in cellular excitability.

Mechanism from Hyper- to Hypoinsulin Secretion

Changes from hyperinsulin secretion to hypoinsulin secretion were seen in islets from the young (3 weeks) and the middle-age (30 weeks) KO mice. In the young mouse islet cells, a high basal level of intracellular calcium was seen (Figure 7A). Consistently, high insulin secretion was seen in response to high glucose stimulation (Figure 7B). However, blunted intracellular calcium elevation (Figure 7A) and dysfunction of insulin secretion (Figure 7B) were seen in response to high glucose stimulation in the middle-age mice. Insulin content was unchanged at 3 and 30 weeks (Figure 7C). Western blot showed that the KO mouse islet had decreased proliferation, increased endoplasmic reticulum (ER) stress, and apoptosis in the middle-age mice (Figure 7D). The islet β cell mass in the KO mice was decreased at 30 weeks. Immunocytochemistry analysis indicated a reduction in insulin staining and an increase in glucagon-staining cells within the core of the islet (Figure 7E). Immunochemistry also showed an increased ER stress (Figure 7F) and apoptosis

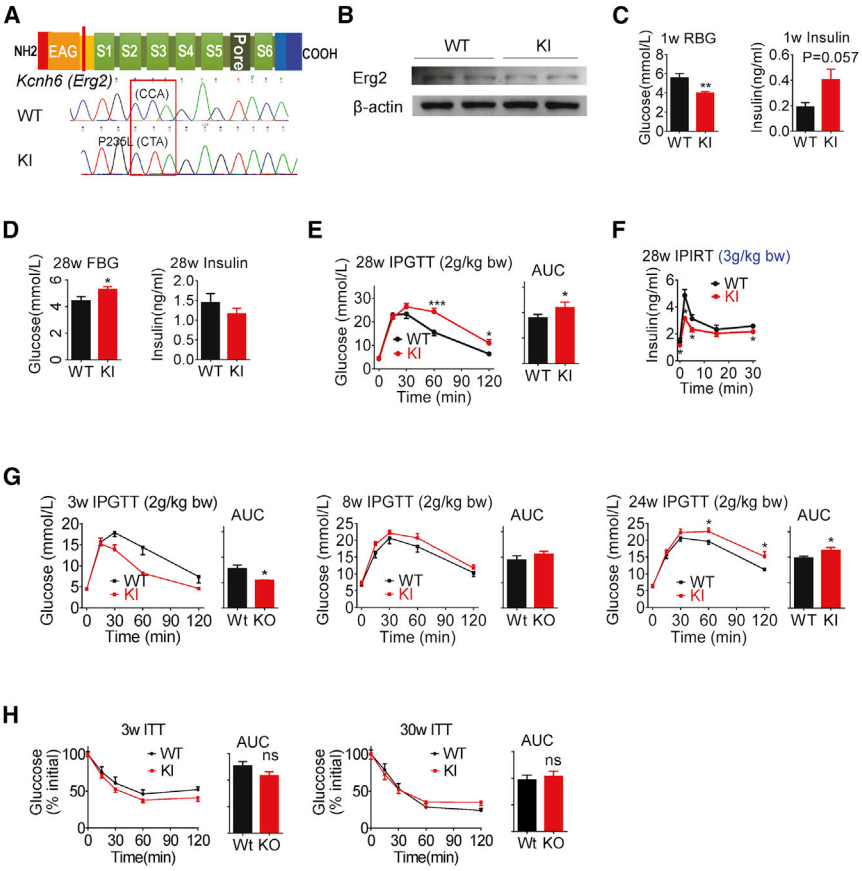

Figure 5. Mice with Cas9-Mediated Kcnh6 p.P235L KI Exhibited the Diabetes 2 Phenotype

(A) Genotypes and DNA sequences of WT and Kcnh6 p.P235L knockin (KI).

(B) Western blot analysis for Kcnh6 protein in WT and KI mouse islets.

(C) Random blood glucose (RBG) (WT, n = 8; KI, n = 6) and plasma insulin (WT, n = 3; KI, n = 5) in neonatal KI and WT mice.

(D) Fasting insulin and glucose at week 28 (WT, n = 6; KI, n = 8).

(E) Blood glucose levels and area under the curve (AUC) during an intraperitoneal glucose tolerance test (IPGTT) (3 g glucose/kg bw) at week 28 (WT, n = 9; KI, n = 11).

(F) First- and second-phase insulin secretory responses to glucose IPGTT (3 g glucose/kg bw) at week 28 (WT, n = 9; KI, n = 11).

(G) Consecutive plasma glucose levels and area under the curve (AUC) during ITT (2 g glucose/kg bw) at weeks 3, 8, and 24 (WT, n = 7; KI, n = 7).

(H) Consecutive plasma glucose levels and area under the curve (AUC) during ITT (2 g glucose/kg bw) at weeks 3 and 30 (WT, n = 8; KI, n = 8).

Values represent means ± SEM. *p < 0.05, **p < 0.01, ***p < 0.001 versus WT. Significance values were calculated using Student's unpaired t test or the Mann-Whitney U test if n < 9.

(Figure 7G) of islet cells from the KO mice at 30 weeks. Acridine orange/propidium iodide (AO/PI) staining showed that dead islet cells were elevated in the KO mice at 30 weeks (Figure 7H).

DISCUSSION

Our results indicate that hyperinsulin secretion and subsequent hypoinsulin secretion caused by KCNH6 K^+ channel dysfunction in humans and mice are a result of overstimulation of insulin secretion. KCNH6 loss-of-function causes ultra-high intracellular calcium concentration and super-high insulin secretion in the short term. In the long term, this ultra-high calcium concentration and overstimulation of insulin release may cause ER stress, apoptosis, loss of β cell mass, and subsequent decreased insulin secretions. Increased intracellular calcium levels have toxic effects, leading to cell death (Gyengesi et al., 2012). In addition, ER stress and apoptosis of islet cells may be caused by chronic overstimulation of insulin secretion (Glaser et al., 1999; Liang et al., 2014). Based on the calcium stress hypothesis, overstimulation of insulin secretion appears to be a double-edged sword. It may cause not only hyperinsulinemia in the short term but also β cell failure in the long term (Efanova et al., 1998). Therefore, KCNH6 Mut results in phenotype changing from hyper- to hypoinsulinemia and diabetes.

Consistent with this overstimulation and calcium stress hypothesis, Muts in K_{ATP} channel genes (*ABCC8* and *KCNJ11*) can cause either hyperinsulinemia or dysfunction of insulin secretion with diabetes (Kapoor et al., 2011). A study of a large Finnish family described how a dominant W/m p.E1506K Mut in *ABCC8* caused congenital hyperinsulinemia in infancy, loss of insulin secretory capacity in early adulthood, and diabetes in middle age (Huopio et al., 2003). In another family, a W/m E1506K Mut in *ABCC8* was associated with persistent hypoglycemia in the neonatal period and diabetes in adulthood (Vieira et al., 2010). A Mut in *KCNJ11* (p.Y12X) was known to cause human hyperinsulinemia, and an interesting study showed that this Mut resulted in a glucose-intolerant phenotype in mice (Hugill et al., 2010).

We know that MODY prevalence is low, and we should be cautious to interpret KCNH6 p.P235L Mut as the cause of a new MODY Mut. Of hyperglycemic adults diagnosed as having T2D, 3% are affected by multigenerational monogenic diabetes (Ludovico et al., 2015; Pezzilli et al., 2018). Usually, these patients present with the typical of metabolic abnormalities observed in T2D. In these patients, age at diagnosis is older than the age of patients with MODY but younger than the age of patients with classic T2D (Ludovico et al., 2015; Pezzilli et al., 2018).

We showed the staining of KCNH6 was not restricted to plasma membrane. It appears that KCNH K^+ channels should be localized to plasma membrane. However, as previously reported, the staining of KCNH-class channels was not restricted to plasma membrane but rather was diffused throughout cytosol (Li et al., 2014; Tanaka et al., 2014; Uhlén et al., 2015). KCNH6 is also expressed in α cells, and it is surprising that glucagon

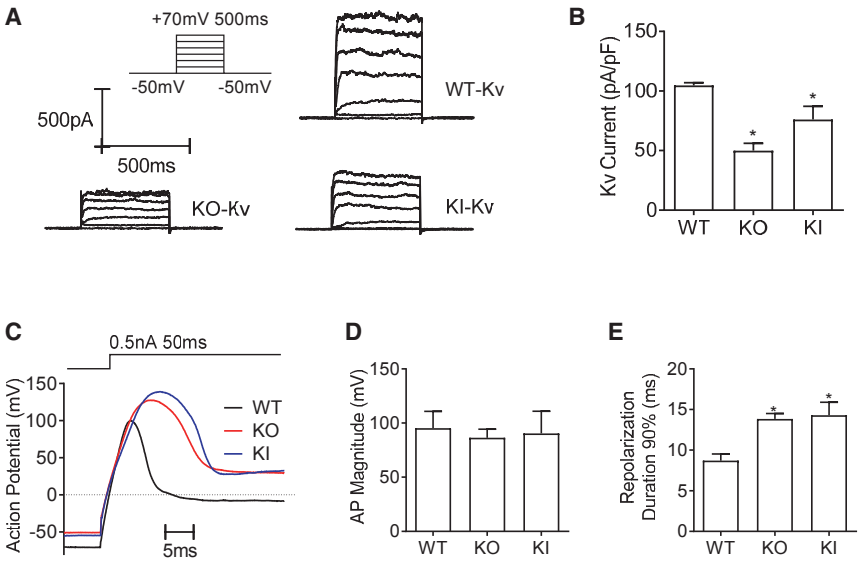

Figure 6. Kv Current and Action Potential of Mouse Pancreatic β Cells

(A and B) Voltage-dependent K^+ (Kv) channels of mouse pancreatic β cells.

(A) Representative currents of WT, KO, and KI.

(B) Summary of the mean current density of Kv channels at +70 mV (KO, n = 5; KI, n = 7; WT, n = 3).

(C–E) Action potential of mouse pancreatic β cells.

(C) Action potential evoked by a 0.5 nA current.

(D) Action potential magnitude of KO (n = 3), KI (n = 3), and WT (n = 4).

(E) 90% of action potential duration of KO (n = 3), KI (n = 3), and WT (n = 6).

Values represent means ± SEM. *p < 0.05 versus WT. Significance values were calculated using the Mann-Whitney U test.

secretion is unaltered in this study. The reason may be that although KCNH2 and KCNH6 are present in both α and β cells, KCNH6 is relatively dominant in β cells, while KCNH2 is dominant in α cells (Hardy et al., 2009). Therefore, KCNH6 current may not be a dominant Kv current for glucagon secretion in α cells.

This study focused on finding the role of KCNH6 in insulin secretion. The clinical data supporting KCNH6 Mut as a new type of MODY are not strong and only give us a clue for further investigation. Although many subtypes of Kv channels have been detected in islet β cells (Félix-Martínez and Godínez-Fernández, 2014; Yang et al., 2014), and some studies have investigated the contribution of Kv channels to membrane repolarization in β cells (Rorsman and Braun, 2013; Rosati et al., 2000), little was known about which Kv channel is the main regulator responsible for β cell repolarization and insulin secretion. This may due to the lack of channel-blocking agents specific for each Kv channel. Whether the Kv-related KCNH6 channel is as a major contributor to outward Kv currents for regulating insulin secretion and a promising antidiabetic target needs to be studied further.

Filling the knowledge gap on monogenic diabetes genes would be extremely useful for etiological mechanisms, as well as novel treatment approaches for diabetes. An example of this usefulness relates to the K_{ATP} channel. This channel has been exploited for the development of insulin secretagogues for more than 60 years, including sulfonylureas and glinides treating T2D and some types of monogenic diabetes (Pearson et al., 2006).

STAR★METHODS

Detailed methods are provided in the online version of this paper and include the following:

- KEY RESOURCES TABLE
- CONTACT FOR REAGENT AND RESOURCE SHARING
- EXPERIMENTAL MODEL AND SUBJECT DETAILS
  - Patients
  - Cell culture
  - Animal Model and Animal Care
- METHOD DETAILS
  - Clinical and biochemical parameters
  - Oral glucose tolerance test (OGTT)
  - Classification of glucose homeostasis
  - Insulin resistance and β-cell function
  - Exome sequencing and bioinformatics analysis
  - Real-time PCR
  - Site-directed mutagenesis of human KCNH6 and HEK293 cell transfection
  - Immunohistochemistry
  - Patch-Clamp experiment of KCNH6 in HEK293 cells and pancreas β-cells
  - Co-immunoprecipitation
  - Kcnh6 knockdown in INS-1 β-cells
  - Intraperitoneal Glucose tolerance test (IPGTT), intraperitoneal insulin releasing test (IPIRT) and Insulin tolerance test (ITT)
  - Isolation of mice pancreatic islets
  - Glucose-stimulated insulin secretion (GSIS)
  - Western blot
  - β-Cell Mass Quantification
  - Total pancreas insulin content
  - Intracellular Calcium Level Measurement
- QUANTIFICATION AND STATISTICAL ANALYSIS
  - Data analysis
- DATA AND SOFTWARE AVAILABILITY
  - Data Resources

SUPPLEMENTAL INFORMATION

Supplemental Information includes nine figures and five tables and can be found with this article online at https://doi.org/10.1016/j.celrep.2018.12.005.

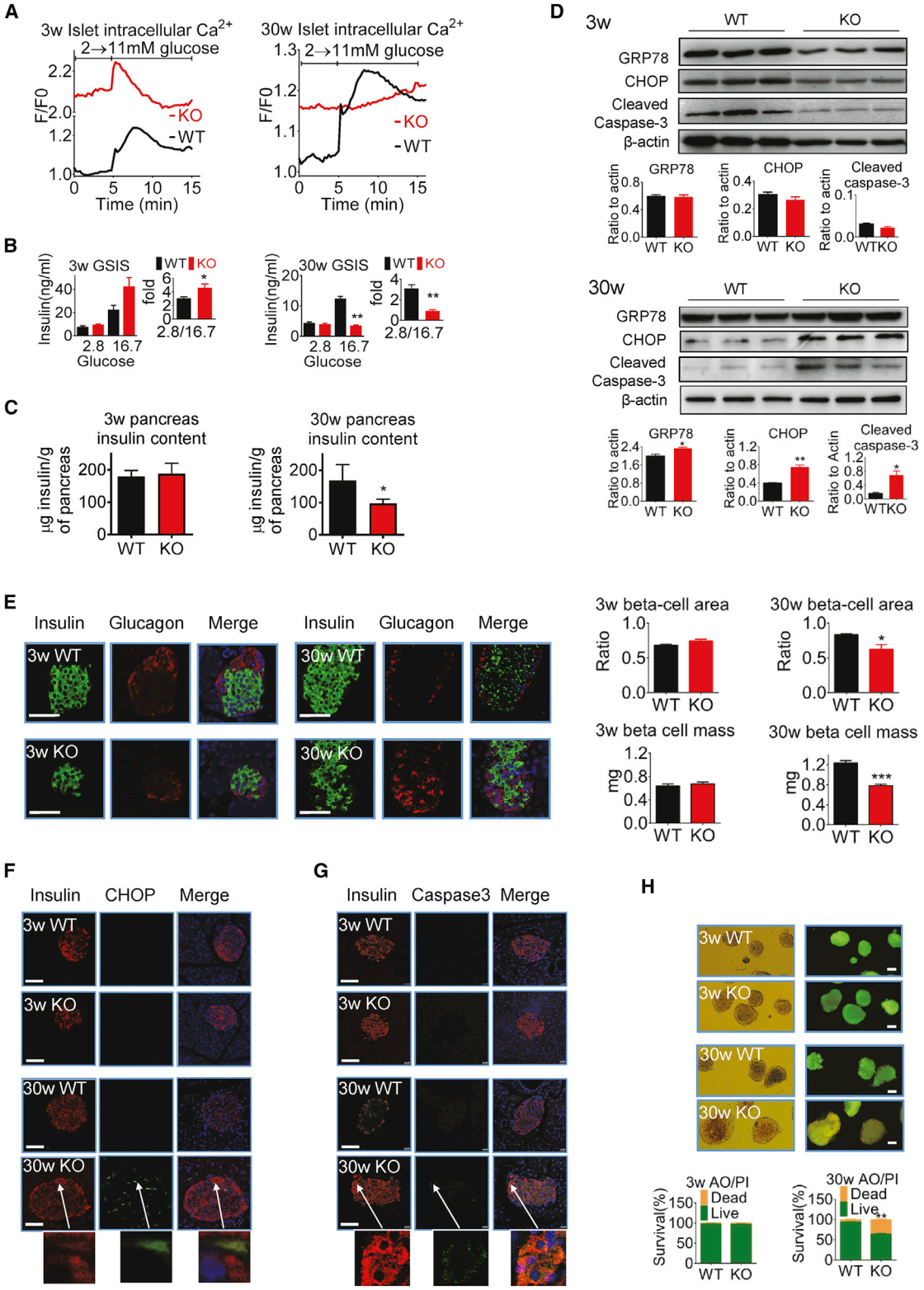

Figure 7. Islets from Young and Middle-Age Mice with *Kcnh6* KO Exhibit Changes from Hyper- to Hypoinsulin Secretion with Concomitant ER Stress and Apoptosis

(A–C) Islet cell parameters including glucose-stimulated intracellular calcium mean level (A) (n = 3 β cells per group), glucose-stimulated insulin secretion (GSIS; B) (n = 60 islets from 4 mice per group), and total pancreas insulin content (C) (n = 3–5 mice per group) from 3- or 30-week-old mice.

(legend continued on next page)

ACKNOWLEDGMENTS

This work was supported by grants from the National Natural Science Foundation of China (81471014 and 81561128015) and National Key R&D Program of China (2017YFC0909600) to J.-K.Y., the National Natural Science Foundation of China (81800688) to J.L., the National Natural Science Foundation of China (81471009) to G.-R.Y., and the National 973 Program of China (2015CB942803) to B.Z. We thank Core Facilities Center of Capital Medical University for the support of this work.

AUTHOR CONTRIBUTIONS

J.-K.Y. conceived the idea for the study, designed the experiments, performed the experiments, and wrote the manuscript. J.L., S.-S.Y., and A. designed and performed the experiments. X.C., H.-Y.Q., T.-T.S., F.-Y.Y., Q.L., Q.W., Y.-H.W., H.-X.H., A.K., M.-R.Z., and C.-L.X. performed the experiments. C.-P.L., J.-P.F., R.-R.X., X.-R.Z., C.L., and G.-R.Y. performed the clinical work. C.C., B.Z., G.L., X.-Q.Z., and A.X. helped with the interpretation of the results and approved the final version of the manuscript.

DECLARATION OF INTERESTS

The authors declare no competing interests.

Received: May 17, 2017
Revised: June 26, 2018
Accepted: November 30, 2018
Published: December 26, 2018

REFERENCES

Bonnefond, A., Philippe, J., Durand, E., Dechaume, A., Huyvaert, M., Montagne, L., Marre, M., Balkau, B., Fajardy, I., Vambergue, A., et al. (2012). Whole-exome sequencing and high throughput genotyping identified KCNJ11 as the thirteenth MODY gene. PLoS ONE *7*, e37423.

Bowman, P., Flanagan, S.E., Edghill, E.L., Damhuis, A., Shepherd, M.H., Paisey, R., Hattersley, A.T., and Ellard, S. (2012). Heterozygous ABCC8 mutations are a cause of MODY. Diabetologia *55*, 123–127.

Braun, M., Ramracheya, R., Bengtsson, M., Zhang, Q., Karanauskaite, J., Partridge, C., Johnson, P.R., and Rorsman, P. (2008). Voltage-gated ion channels in human pancreatic beta-cells: electrophysiological characterization and role in insulin secretion. Diabetes *57*, 1618–1628.

Brouwers, B., de Faudeur, G., Osipovich, A.B., Goyvaerts, L., Lemaire, K., Boesmans, L., Cauwelier, E.J., Granvik, M., Pruniau, V.P., Van Lommel, L., et al. (2014). Impaired islet function in commonly used transgenic mouse lines due to human growth hormone minigene expression. Cell Metab *20*, 979–990.

Efanova, I.B., Zaitsev, S.V., Zhivotovsky, B., Köhler, M., Efendić, S., Orrenius, S., and Berggren, P.O. (1998). Glucose and tolbutamide induce apoptosis in pancreatic beta-cells. A process dependent on intracellular Ca2+ concentration. J. Biol. Chem. *273*, 33501–33507.

Félix-Martínez, G.J., and Godínez-Fernández, J.R. (2014). Mathematical models of electrical activity of the pancreatic β-cell: a physiological review. Islets *6*, e949195.

Gao, R., Liu, Y., Gjesing, A.P., Hollensted, M., Wan, X., He, S., Pedersen, O., Yi, X., Wang, J., and Hansen, T. (2014). Evaluation of a target region capture sequencing platform using monogenic diabetes as a study-model. BMC Genet. *15*, 13.

Glaser, B., Ryan, F., Donath, M., Landau, H., Stanley, C.A., Baker, L., Barton, D.E., and Thornton, P.S. (1999). Hyperinsulinism caused by paternal-specific inheritance of a recessive mutation in the sulfonylurea-receptor gene. Diabetes *48*, 1652–1657.

Guo, J.H., Chen, H., Ruan, Y.C., Zhang, X.L., Zhang, X.H., Fok, K.L., Tsang, L.L., Yu, M.K., Huang, W.Q., Sun, X., et al. (2014). Glucose-induced electrical activities and insulin secretion in pancreatic islet β-cells are modulated by CFTR. Nat. Commun. *5*, 4420.

Gyengesi, E., Paxinos, G., and Andrews, Z.B. (2012). Oxidative stress in the hypothalamus: the importance of calcium signaling and mitochondrial ROS in body weight regulation. Curr. Neuropharmacol. *10*, 344–353.

Haitin, Y., Carlson, A.E., and Zagotta, W.N. (2013). The structural mechanism of KCNH-channel regulation by the eag domain. Nature *501*, 444–448.

Hardy, A.B., Fox, J.E., Giglou, P.R., Wijesekara, N., Bhattacharjee, A., Sultan, S., Gyulkhandanyan, A.V., Gaisano, H.Y., MacDonald, P.E., and Wheeler, M.B. (2009). Characterization of Erg K+ channels in alpha- and beta-cells of mouse and human islets. J. Biol. Chem. *284*, 30441–30452.

Horikawa, Y., Iwasaki, N., Hara, M., Furuta, H., Hinokio, Y., Cockburn, B.N., Lindner, T., Yamagata, K., Ogata, M., Tomonaga, O., et al. (1997). Mutation in hepatocyte nuclear factor-1 beta gene (TCF2) associated with MODY. Nat. Genet. *17*, 384–385.

Houamed, K.M., Sweet, I.R., and Satin, L.S. (2010). BK channels mediate a novel ionic mechanism that regulates glucose-dependent electrical activity and insulin secretion in mouse pancreatic β-cells. J. Physiol. *588*, 3511–3523.

Hugill, A., Shimomura, K., Ashcroft, F.M., and Cox, R.D. (2010). A mutation in KCNJ11 causing human hyperinsulinism (Y12X) results in a glucose-intolerant phenotype in the mouse. Diabetologia *53*, 2352–2356.

Huopio, H., Otonkoski, T., Vauhkonen, I., Reimann, F., Ashcroft, F.M., and Laakso, M. (2003). A new subtype of autosomal dominant diabetes attributable to a mutation in the gene for sulfonylurea receptor 1. Lancet *361*, 301–307.

Hyltén-Cavallius, L., Iepsen, E.W., Wewer Albrechtsen, N.J., Svendstrup, M., Lubberding, A.F., Hartmann, B., Jespersen, T., Linneberg, A., Christiansen, M., Vestergaard, H., et al. (2017). Patients with long-QT syndrome caused by impaired *hERG*-encoded K_v11.1 potassium channel have exaggerated endocrine pancreatic and incretin function associated with reactive hypoglycemia. Circulation *135*, 1705–1719.

Kapoor, R.R., Flanagan, S.E., James, C.T., McKiernan, J., Thomas, A.M., Harmer, S.C., Shield, J.P., Tinker, A., Ellard, S., and Hussain, K. (2011). Hyperinsulinaemic hypoglycaemia and diabetes mellitus due to dominant ABCC8/KCNJ11 mutations. Diabetologia *54*, 2575–2583.

Li, G., Cheng, G., Wu, J., Ma, S., Zhang, A., Han, W., and Sun, C. (2014). Allitridin reduces I Kr current by disrupting the trafficking of human ether-à-go-go-related gene channels. Cardiology *128*, 1–8.

Li, Q., Cao, X., Qiu, H.Y., Lu, J., Gao, R., Liu, C., Yuan, M.X., Yang, G.R., and Yang, J.K. (2016). A three-step programmed method for the identification of causative gene mutations of maturity onset diabetes of the young (MODY). Gene *588*, 141–148.

(D) Western blot of GRP78 and CHOP (for representing ER stress), and cleaved caspase-3 (for representing apoptosis) of islets from 3- or 30-week-old mice (WT and KO, n = 600 islets from 6 mice per group).
(E) Insulin and glucagon immunohistochemistry for β cell mass and β cell area of islets from 3- or 30-week-old mice (WT and KO, n = 4 mice per group).
(F) CHOP immunohistochemistry for ER stress of islets from 3- or 30-week-old mice (WT and KO, n = 600 islets from 6 mice per group).
(G) Caspase-3 immunohistochemistry for cell apoptosis of islets from 3- or 30-week-old mice (WT and KO, n = 6 mice per group).
(H) AO/PI staining for cell viability of islets from 3- or 30-week-old mice (WT and KO, n = 120 islets from 6 mice per group). Red islet cells are dead, and green islet cells are alive.
All scale bars in white are 50 μm in length. Values represent means ± SEM. *$p < 0.05$, **$p < 0.01$ versus WT. Significance values were calculated using the Mann-Whitney U test.

Liang, K., Du, W., Lu, J., Li, F., Yang, L., Xue, Y., Hille, B., and Chen, L. (2014). Alterations of the Ca^{2+} signaling pathway in pancreatic beta-cells isolated from db/db mice. Protein Cell *5*, 783–794.

Ludovico, O., Carella, M., Bisceglia, L., Basile, G., Mastroianno, S., Palena, A., De Cosmo, S., Copetti, M., Prudente, S., and Trischitta, V. (2015). Identification and clinical characterization of adult patients with multigenerational diabetes mellitus. PLoS ONE *10*, e0135855.

MacDonald, P.E., Ha, X.F., Wang, J., Smukler, S.R., Sun, A.M., Gaisano, H.Y., Salapatek, A.M., Backx, P.H., and Wheeler, M.B. (2001). Members of the Kv1 and Kv2 voltage-dependent K(+) channel families regulate insulin secretion. Mol. Endocrinol. *15*, 1423–1435.

MacDonald, P.E., Sewing, S., Wang, J., Joseph, J.W., Smukler, S.R., Sakellaropoulos, G., Wang, J., Saleh, M.C., Chan, C.B., Tsushima, R.G., et al. (2002). Inhibition of Kv2.1 voltage-dependent K+ channels in pancreatic beta-cells enhances glucose-dependent insulin secretion. J. Biol. Chem. *277*, 44938–44945.

Mühlbauer, E., Bazwinsky, I., Wolgast, S., Klemenz, A., and Peschke, E. (2007). Circadian changes of ether-a-go-go-related-gene (Erg) potassium channel transcripts in the rat pancreas and beta-cell. Cell. Mol. Life Sci. *64*, 768–780.

Niu, M.J., Yang, J.K., Lin, S.S., Ji, X.J., and Guo, L.M. (2008). Loss of angiotensin-converting enzyme 2 leads to impaired glucose homeostasis in mice. Endocrine *34*, 56–61.

Pearson, E.R., Flechtner, I., Njolstad, P.R., Malecki, M.T., Flanagan, S.E., Larkin, B., Ashcroft, F.M., Klimes, I., Codner, E., Iotova, V., et al. (2006). Switching from insulin to oral sulfonylureas in patients with diabetes due to Kir6.2 mutations. N. Engl. J. Med *355*, 467–477.

Pezzilli, S., Ludovico, O., Biagini, T., Mercuri, L., Alberico, F., Lauricella, E., Dallali, H., Capocefalo, D., Carella, M., Miccinilli, E., et al. (2018). Insights from molecular characterization of adult patients of families with multigenerational diabetes. Diabetes *67*, 137–145.

Proverbio, M.C., Mangano, E., Gessi, A., Bordoni, R., Spinelli, R., Asselta, R., Valin, P.S., Di Candia, S., Zamproni, I., Diceglie, C., et al. (2013). Whole genome SNP genotyping and exome sequencing reveal novel genetic variants and putative causative genes in congenital hyperinsulinism. PLoS ONE *8*, e68740.

Rorsman, P., and Braun, M. (2013). Regulation of insulin secretion in human pancreatic islets. Annu. Rev. Physiol *75*, 155–179.

Rosati, B., Marchetti, P., Crociani, O., Lecchi, M., Lupi, R., Arcangeli, A., Olivotto, M., and Wanke, E. (2000). Glucose- and arginine-induced insulin secretion by human pancreatic beta-cells: the role of HERG K(+) channels in firing and release. FASEB J *14*, 2601–2610.

Sanguinetti, M.C., Jiang, C., Curran, M.E., and Keating, M.T. (1995). A mechanistic link between an inherited and an acquired cardiac arrhythmia: HERG encodes the IKr potassium channel. Cell *81*, 299–307.

Segerstolpe, Å., Palasantza, A., Eliasson, P., Andersson, E.M., Andréasson, A.C., Sun, X., Picelli, S., Sabirsh, A., Clausen, M., Bjursell, M.K., et al. (2016). Single-cell transcriptome profiling of human pancreatic islets in health and type 2 diabetes. Cell Metab. *24*, 593–607.

Shi, W., Wymore, R.S., Wang, H.S., Pan, Z., Cohen, I.S., McKinnon, D., and Dixon, J.E. (1997). Identification of two nervous system-specific members of the erg potassium channel gene family. J. Neurosci. *17*, 9423–9432.

Tanaka, H., Takahashi, Y., Hamaguchi, S., Iida-Tanaka, N., Oka, T., Nishio, M., Ohtsuki, A., and Namekata, I. (2014). Effect of terfenadine and pentamidine on the HERG channel and its intracellular trafficking: combined analysis with automated voltage clamp and confocal microscopy. Biol. Pharm. Bull. *37*, 1826–1830.

Thanabalasingham, G., and Owen, K.R. (2011). Diagnosis and management of maturity onset diabetes of the young (MODY). BMJ *343*, d6044.

Uhlén, M., Fagerberg, L., Hallström, B.M., Lindskog, C., Oksvold, P., Mardinoglu, A., Sivertsson, Å., Kampf, C., Sjöstedt, E., Asplund, A., et al. (2015). Proteomics. Tissue-based map of the human proteome. Science *347*, 1260419.

Vieira, T.C., Bergamin, C.S., Gurgel, L.C., and Moisés, R.S. (2010). Hyperinsulinemic hypoglycemia evolving to gestational diabetes and diabetes mellitus in a family carrying the inactivating ABCC8 E1506K mutation. Pediatr. Diabetes *11*, 505–508.

Vionnet, N., Stoffel, M., Takeda, J., Yasuda, K., Bell, G.I., Zouali, H., Lesage, S., Velho, G., Iris, F., Passa, P., et al. (1992). Nonsense mutation in the glucokinase gene causes early-onset non-insulin-dependent diabetes mellitus. Nature *356*, 721–722.

Yamagata, K., Furuta, H., Oda, N., Kaisaki, P.J., Menzel, S., Cox, N.J., Fajans, S.S., Signorini, S., Stoffel, M., and Bell, G.I. (1996a). Mutations in the hepatocyte nuclear factor-4alpha gene in maturity-onset diabetes of the young (MODY1). Nature *384*, 458–460.

Yamagata, K., Oda, N., Kaisaki, P.J., Menzel, S., Furuta, H., Vaxillaire, M., Southam, L., Cox, R.D., Lathrop, G.M., Boriraj, V.V., et al. (1996b). Mutations in the hepatocyte nuclear factor-1alpha gene in maturity-onset diabetes of the young (MODY3). Nature *384*, 455–458.

Yang, S.N., Shi, Y., Yang, G., Li, Y., Yu, J., and Berggren, P.O. (2014). Ionic mechanisms in pancreatic β cell signaling. Cell. Mol. Life Sci. *71*, 4149–4177.

Zmuda, E.J., Powell, C.A., and Hai, T. (2011). A method for murine islet isolation and subcapsular kidney transplantation. J. Vis. Exp. *50*, 2096.

Zu, Y., Tong, X., Wang, Z., Liu, D., Pan, R., Li, Z., Hu, Y., Luo, Z., Huang, P., Wu, Q., et al. (2013). TALEN-mediated precise genome modification by homologous recombination in zebrafish. Nat. Methods *10*, 329–331.

STAR★METHODS

KEY RESOURCES TABLE

REAGENT or RESOURCE	SOURCE	IDENTIFIER
Antibodies		
Goat anti-human insulin antibody	Santa-Cruz Biotechnology	Cat# SC-7839; RRID: AB_2296108
Mouse monoclonal anti-glucagon antibody	Sigma	Cat# G2654; RRID: AB_259852
Rabbit anti-mouse insulin antibody	Cell signaling Technology	Cat# 4590; RRID: AB_659820
Rabbit anti-human KCNH6 antibody	Sigma	Cat# SAB2104242; RRID: SAB2104242
Alexa Fluor 555 mouse anti-goat IgG-CFL	Santa-Cruz Biotechnology	Cat# SC-362267; RRID: AB_10986269
Alexa Fluor 555 donkey anti-mouse IgG-CFL	Santa-Cruz Biotechnology	Cat# SC-362268; RRID: AB_10987655
Alexa Fluor 488 goat anti-rabbit Cy2	Abcam	Cat# ab150081; RRID: AB_2734747
Mouse monoclonal anti-Flag antibody	Sigma	Cat# F3165; RRID: AB_259529
Anti-Myc antibody	Cell signaling Technology	Cat# 2278S; RRID: AB_10693332
horseradish peroxidase (HRP)-labeled donkey-anti Rabbit IgG	Santa-Cruz Biotechnology	Cat# SC2305; RRID: AB_641180
Rabbit anti-Caspase3 antibody	Cell signaling Technology	Cat# 9662; RRID: AB_331439
Mouse anti-CHOP antibody	Cell signaling Technology	Cat#2895; RRID: AB_2089254
Rabbit polyclonal anti-GRP78 antibody	Abcam	Cat#ab32618; RRID: AB_732737
Rabbit polyclonal anti-β-actin antibody	Cell signaling Technology	Cat#58169; RRID: AB_2750839
Bacterial and Virus Strains		
Subcloning Efficiency DH5α Competent Cells	Invitrogen	Cat# 18265017
Biological Samples		
Human blood samples	Donated from the patients, Beijing Tongren Hospital, Capital Medical University	http://www.trhos.com
Human pancreatic tissues	Donated from Pathology department of Beijing Tongren Hospital, Capital Medical University	http://www.trhos.com
Chemicals, Peptides, and Recombinant Proteins		
Calcium Orange	Thermo	Cat# C3015
Pluronic F-127	Thermo	Cat# P3000MP
Anti-Flag M2 affinity gel	Sigma	Cat# A2220; RRID: AB_10063035
DMEM	GIBCO	Cat# 11965-092
Fetal bovine serum	GIBCO	Cat# 10099-141
HBSS	Invitrogen	Cat# 14175103
Ficoll PM 400	Sigma	Cat# F4375
BSA	Sigma	Cat# B2064
RPMI1640	GIBCO	Cat# 12633-012
Penicillin–streptomycin, liquid	Invitrogen	Cat# 15140122
Lipofectamine 2000	Invitrogen	Cat# 11668019
LightCycler 480 SYBR Green	Roche	Cat# 4887352001
FastQuant RT Super Mix	Tiangen Biotech	Cat# KR108
Enzyme free cell dissociation solution	Millipore	Cat# S-004-B
ECL Western Blotting Substrate	Bio-rad	Cat# 1705060
Critical Commercial Assays		
TIANapm blood DNA MIDI kit	Tiangen Biotech	Cat# DP332
TIANamp Blood Genomic DNA Purification Kit	Tiangen Biotech	Cat# DP304
RNAprep pure Tissue Kit	Tiangen Biotech	Cat# DP431

(*Continued on next page*)

Continued

REAGENT or RESOURCE	SOURCE	IDENTIFIER
SP6 mMESSAGE mMACHINE Kit	Thermo	Cat# AM1340
Plasma Membrane protein isolation kit	Invent Biochnologies	Cat# SM-005
GLP-1 Elisa kit	Millipore	Cat# EGLP-35K
Glucagon Quantikine ELISA kit	R&D	Cat# DGCG0
Insulin Elisa kit for Rat/Mouse	Millipore	Cat# EZRMI-13K
Deposited Data		
Raw and analyzed data	This paper	SRA: PRJNA506803
Human reference genome UCSC build 37, version 19	Genome Reference Consortium	http://genome.ucsc.edu
Experimental Models: Cell Lines		
Human: HEK293 cell lines	Cell resource center, Chinese Academy of Medical Science	http://www.crcpumc.com/pd.jsp?id=592#keyword=293T&_pp=0_312
Rat: INS-1E cell lines	Cell resource center, Chinese Academy of Medical Science	http://www.crcpumc.com/pd.jsp?id=776#keyword=INS-1&_pp=0_312
Experimental Models: Organisms/Strains		
Mouse:C57BL/6N	Vital River Laboratories	http://www.vitalriver.com/proinfo.aspx?nid=41
Mouse: Kcnh6 KO	This paper	N/A
Mouse: Kcnh6 P245L KI	This paper	N/A
Oligonucleotides		
Primer for KCNH2; Forward:ACACGGCTGTCTTCACACCCTACT	This paper	N/A
Primer for KCNH2; Reverse:CTGACCACCTCCTCGTTGGCATT	This paper	N/A
Primer for KCNH6; Forward: TCTCGCCCAACACCAACTC	This paper	N/A
Primer for KCNH6; Reverse: AGCGGATGAACTCCTTGACAC	This paper	N/A
Primer for KCNH7; Forward: CAAACCTCAACAAATACAGCACCAT	This paper	N/A
Primer for KCNH7; Reverse: ACCAACAGCAGGATAAGCCAGTC	This paper	N/A
Primer for TALEN target site; Forward: CTGCTCTCTCCCTCTGTCCT	This paper	N/A
Primer for TALEN target site; Reverse: GGTATAGCCGCAGGTACCAC	This paper	N/A
Primer for Cas9 target site; Forward: TGCCTTTCATGACTGTGACA	This paper	N/A
Primer for Cas9 target site; Reverse: CGGTGCCTGCAGCTTGTACT	This paper	N/A
The sequence of Cas9 designed for Kcnh6 point; Mut: CTGCTAGGAAGACCGGTCTA TGG	This paper	N/A
Recombinant DNA		
Plasmid: GV314-EGFP	GeneChem	N/A
Plasmid: EGFP-KCNH6	This paper	N/A
Plasmid: EGFP-KCNH6-Site Mut	This paper	N/A
shRNA of mouse Kcnh6:	Origene	Cat#: TF512772
Plasmid: pCS2-FokI	Zu et al., 2013	N/A
Software and Algorithms		
Prism 7	Graphpad	https://www.graphpad.com
Version 11.4	MedCalc	http://www.medcalc.com
Version 1	MutationTaster	http://www.mutationtaster.org/

(*Continued on next page*)

Continued

REAGENT or RESOURCE	SOURCE	IDENTIFIER
Version 2	PolyPhen	http://genetics.bwh.harvard.edu/pph2/
ImageJ	NIH	https://imagej.nih.gov/ij/

CONTACT FOR REAGENT AND RESOURCE SHARING

Further information and requests for resources and reagents should be directed to and will be fulfilled by the Lead Contact, Dr. Jin-Kui Yang (jkyang@ccmu.edu.cn).

EXPERIMENTAL MODEL AND SUBJECT DETAILS

Patients

Clinically suspected MODY: Screening criteria for MODY were based on the algorithm described previously (Thanabalasingham and Owen, 2011). Those patients with a family history of diabetes for at least two generations, with an age of diagnosis between 14 and 30 years, and absence of insulin resistance were eligible.

This study was approved by the Ethics Committee of Beijing Tongren Hospital, Capital Medical University and performed according to the principles of the Declaration of Helsinki II. We obtained written informed consent from each participant, and we got it from the next of kin on the behalf of the minors/children taking part in this study.

Cell culture

Human embryonic kidney (HEK) 293 cells and INS-1 β-cells were cultured in a humidified atmosphere containing 5% CO_2 provided by Cell Resource Center, Chinese Academy of Medical Sciences (Beijing, China). HEK293 were cultured in Dulbecco's modified Eagle's medium (DMEM) supplemented with 10% fetal bovine serum (FBS) and 1% penicillin–streptomycin. INS-1 β-cells were cultured in RPMI-1640 (GIBCO) supplemented with 10% fetal bovine serum, 1 mM sodium pyruvate, 50 mM 2-mercaptoethanol, 2 mM glutamine, 10 mM HEPES, 1% penicillin–streptomycin.

Animal Model and Animal Care

Male C57BL/6N mice were purchased from Vital River Laboratories (Beijing, China). The mice were kept at constant temperature and humidity, with a 12 hr light and dark cycle, and fed a regular unrestricted diet. Both male and female mice were used in our experiment, and we did not find any sex-based differences.

Mice with *Kcnh6* KO were generated using our previously reported TALEN method (Zu et al., 2013). A TALEN pair targeting exon 5 of the C57BL/6N mice Erg2 gene was designed (Figure S6A). The binding sites of left and right TALENs' specific for target sequences in Erg2, which are different from other genes (Figure S6B). Approximately 10 ng mRNAs synthesized using the SP6 mMESSAGE mMACHINE Kit (Thermo) encoding each of the two TALENs were injected into the zygotes of C57BL/6N mice. A 382bp genomic DNA fragment containing the target site was amplified using PCR.

We applied the Cas9 system targeting exon 5 of the C57BL/6N mice *Erg2* gene to generate mice with point Muts in *kcnh6*. The sequence of Cas9 is CTGCTAGGAAGACCGGTCTA TGG. mRNA encoding the Cas9 and the synthesized single-strand oligonucleotides donor sequences within P235L point Mut was injected into the zygotes of C57BL/6N mice. A 182 bp genomic DNA fragment containing the target site from injected or control embryos was amplified using PCR.

Animal experiments followed the national ethical guidelines implemented by our institutional Animal Care and Use Committee and were approved by the Ethical Review Committee at the Institute of Zoology, Capital Medical University, China.

METHOD DETAILS

Clinical and biochemical parameters

Medical histories including history of diabetes, diabetes duration and clinical parameters including body mass index (BMI), blood pressure and waist circumference were recorded. Biochemical parameters including fasting plasma glucose (FPG), postprandial plasma glucose (PPG), total cholesterol (TC), triglycerides (TG), low-density lipoprotein (LDL), high-density lipoprotein (HDL) cholesterol, creatinine (Cr), alanine aminotransferase (ALT) and aspartate aminotransferase (AST) were measured by Unicel DXC800 biochemistry analyzer (Beckman Coulter). Glycated hemoglobin A1c (HbA1c) was measured by a high-performance liquid chromatography (HPLC) instrument, VARIANT II (Bio-rad). Insulin and C-peptide were determined using IMMUNLITE-2000 (Siemens). These biochemical measurements had been participated in the Chinese Ministry of Health Quality Assessment Program.

Oral glucose tolerance test (OGTT)

Blood samples were collected after an overnight fast for the determination of plasma glucose and HbA1c levels. After the fasting blood specimen had been taken, a 75 g OGTT was performed between 08:00 and 10:00 hours (h). We took blood samples at 0, 0.5, 1, and 2h for measurement of concentrations of blood glucose, plasma insulin, and plasma C-peptide.

Classification of glucose homeostasis

FPG of $\geq$ 7.0 mmol/l and/or OGTT-120h plasma glucose (2hPG) of $\geq$ 11.1 mmol/l cases were classified as diabetes. Impaired glucose tolerance (IGT) was defined on the basis of FPG < 7.0 mmol/l, 2hPG > 7.8 and < 11.1 mmol/l. Impaired fasting glucose (IFG) was defined as FPG $\geq$ 6.1 and < 7.0 mmol/l, 2hPG < 7.8 mmol/l. FPG of < 6.1 mmol/l and OGTT-120h plasma glucose (2hPG) of < 11.1 mmol/l cases were classified as normal glucose tolerance (NGT).

Insulin resistance and β-cell function

To estimate insulin resistance, HOMA-IR index was calculated as the product of the fasting plasma insulin level (μU/ml) and the fasting plasma glucose level (mmol/l), divided by 22.5. To estimate pancreatic β-cell function, HOMA-β index was calculated as the product of the fasting plasma insulin level (μU/ml) and 20, divided by the fasting plasma glucose level minus 3.5.

Exome sequencing and bioinformatics analysis

Genomic DNA was isolated from peripheral blood leukocytes and sequenced by Sanger sequencing. Captured amplified product is subjected to Hiseq 2000 platform and performed high-throughput sequencing as previously reported (Gao et al., 2014). MutationTaster (http://www.mutationtaster.org/) and PolyPhen-2 (http://genetics.bwh.harvard.edu/pph2/) were used to predict the possible impact of the Muts on protein function.

Real-time PCR

Total RNA was purified using an RNAprep pure Tissue Kit (Tiangen). The RNA samples were converted into cDNA with a FastQuant RT Super Mix (Tiangen). The real-time qPCR was then performed on the LightCycler® 480 Real-Time PCR System (Roche) using SYBR Green I Master Mix reagent (Roche) with the primers.

Site-directed mutagenesis of human KCNH6 and HEK293 cell transfection

The human KCNH6 WT cDNA was subcloned into the GV314-EGFP vector and P235L Mut was constructed by site-directed Mut. The transfection was divided into three groups according to the different plasmids: WT KCNH6 plasmid, P235L Mut plasmid and co-expression of P235L and WT human KCNH6 (WT/Mut) plasmid in a 1:1 ratio. HEK293 cells were transiently transfected using Lipofectamine 2000 reagent (Invitrogen) according to the manufacturer's protocol.

Immunohistochemistry

Human pancreatic tissues donated from the Pathology Department of Beijing Tongren Hospital, Capital Medical University. Human/mouse pancreatic tissues and HEK293 infected with Wt, Mut and Wt/Mut KCNH6 channels were triple-washed with ice-cold PBS. Cells or tissues were fixed by immersion in 4% paraformaldehyde for 4h at room temperature, followed by embedding in paraffin. Heat-induced antigen retrieval then was performed on paraffin-embedded sections (5 μm) by utilizing a microwave in citrate buffer at 99°C for 5 min. Slides were incubated in normal serum at room temperature for 1h, followed by incubation with primary antibody such as insulin antibody (1:100, Santa Cruz Biotechnology), glucagon antibody (1:5000, Sigma), insulin antibody (1:200, Cell Signaling Technology) or KCNH6 antibody (1:200, Sigma) overnight at 4°C. The sections were washed three times with PBS and then were incubated with Alexa Fluor 555 donkey anti-goat-Cy3 (1:200, Santa Cruz Biotechnology), Alexa Fluor 555 donkey anti-mouse IgG-CFL (diluted 1:200, Santa Cruz Biotechnology) or Alexa Fluor 488 goat anti-rabbit-Cy2 (1:200, Abcam) for 45 min at room temperature. These sections were mounted with fluorescent mounting medium containing DAPI. Hematoxylin and Eosin (HE) staining was used to observe the change of islets in morphology. For measurement of pancreatic β-cell area, a minimum of 20 fields per section were assessed using a laser scanning confocal microscope Leica TCSSP5. Captured images from immunohistochemistry with insulin –positive area expect vacuoles were viewed under $_{X}$200 magnifications.

Patch-Clamp experiment of KCNH6 in HEK293 cells and pancreas β-cells

HEK293 cells transiently expressing human KCNH6 were investigated using whole-cell patch clamping to measure the K^+ current through Wt, Mut and Wt/Mut KCNH6 at room temperature. For the experimental current recording, cells were perfused with a Tyrode solution containing (in mmol/l): NaCl 137.0, KCl 4.0, $CaCl_2$ 2.0, $MgCl_2$ 1.0, Glucose 10.0, HEPES 10.0, and the solution was adjusted to pH 7.4 with NaOH. The pipette solution contains (in mmol/l) KCl 130.0, MgATP 5.0, $MgCl_2$ 1.0, EGTA 5.0, HEPES 10.0, and was adjusted to pH 7.3 with KOH. Whole-cell configuration involved use of a glass pipette with tip resistance of 2.5–4.0 MΩ filled with the internal pipette solution. The electrodes were constructed from borosilicate glass using a PB-7 micropipette puller (Narishige Instruments). An EPC-10 patch-clamp amplifier was used with Pulse 8.8 software (HEKA). After cell membrane rupture, at least 5 min was allowed for cell dialysis before any recording.

For Kv channel current recording in mouse pancreas β-cells, the bath solution (in mM) was as follows: NaCl 125, KCl 10, $MgCl_2$ 2, $CaCl_2$ 2, HEPES 10, D-glucose 5.6 with NaOH to pH 7.4. The pipettes were filled with solution (in mM): KCl 130, NaCl 10, $MgCl_2$ 2, $CaCl_2$ 2, EGTA 10, HEPES 10, and ATP-Mg 1 with KOH to pH 7.4. For action potential recording, cells were washed with bath solution containing (in mM): NaCl 130, KCl 5, $MgCl_2$ 1, $CaCl_2$ 2.5, HEPES 20, D-glucose 2.8 with NaOH to pH 7.4. The pipettes were filled with solution (in mM): KCl 138, NaCl 10, $MgCl_2$ 1 and HEPES 10 with KOH to pH 7.4. Action potential is evoked by 0.5 nA current injection.

Co-immunoprecipitation

HEK293 cell lines were transfected with Flag-ERG2 (Wt) and/or Myc-ERG2 P23L Mut. PcDNA3.1 plasmid was used as negative control. Cells were harvested in ice-cold solubilization buffer contained with 10mM HEPES, 50nM NaCl, 5mM EDTA, 1mM benzamidine, 0.5% Triton X-100. Then cells were incubated end-over-end at 4°C for 1h to achieve solubilization. After centrifugation for 15min at 15000 g, supernatants were removed. The solubilizates were then incubated with 25 μL of anti-Flag M2 affinity gel (Sigma) with end-over-end rotation at 4°C overnight. After 6 washes with 1.0 mL of ice-cold solubilization buffer, the immunoprecipitated proteins were eluted from the beads via incubation with SDS-PAGE and visualized via western blot using anti-Flag (Sigma) or anti-Myc (Cell Signaling Technology) antibodies.

Kcnh6 knockdown in INS-1 β-cells

INS-1 β-cells were transfected with shRNA of mouse *Erg2* (OriGene) or scramble shRNA (as a negative control) using Lipofectamine 2000 (Invitrogen). The target sequences are listed as follows: 3′-ACACGCAGATGCTGCGTGTCAAGGAGTTC-5′.

Intraperitoneal Glucose tolerance test (IPGTT), intraperitoneal insulin releasing test (IPIRT) and Insulin tolerance test (ITT)

IPGTT and IPIRT were performed in mice after they fasted overnight for 16 has described previously (Niu et al., 2008). At 0, 15, 30, 60, and 120min after glucose (2g/kg body weight for IPGTT or 3g/kg body weight for IPIRT) injection. For IPGTT about 1 μL blood sample was taken from the angular vein for testing blood glucose concentration using an automatic glucometer ACCU-CHEK® Performa (Roche). For IPIRT about 20 μL blood sample was taken from the angular vein for testing insulin concentrations during IPGTT. Insulin concentration was assayed by an ELISA kit (Millipore). GLP-1 and glucagon were detected using ELISA kit (Millipore and R&D) according to the manufacturer's protocol.

ITT was performed in mice after fasted for 4h. At 0,15, 30, 60, 90, and 120 min after Human regular insulin (Eli Lilly) (0.1 U/ml in saline; 0.75 U/kg body weight) injection, about 1 μL blood sample was taken from the angular vein for testing blood glucose concentration using an automatic glucometer ACCU-CHEK® Performa (Roche).

Isolation of mice pancreatic islets

Pancreatic islets were isolated from overnight-fasted mice by collagenase P (Roche) digestion method (Zmuda et al., 2011). Islets viability was determined by AO/PI staining with living cells stained in green and dead cells stained in red. Isolated islets were incubated in enzyme free cell dissociation solution (Millipore) for 5min and dispersed into a single cell for patch-clamp.

Glucose-stimulated insulin secretion (GSIS)

Islets were preincubated overnight in RPMI 1640 medium. Stably transfected cells were seeded into 24-well plates and incubated for 48 h before GSIS studies were performed. To perform GSIS, groups of 20 islets or cells were washed with krebs-Ringer bicarbonate buffer (KRBB) (129mmol/l NaCl, 4.8mmol/l KCl, 1.2mmol/l $MgSO_4$, 1.2mmol/l KH_2PO_4, 2.5mmol/l $CaCl_2$, 5mmol/l $NaHCO_3$, 0.1% BSA, and 10mmol/l HEPES, PH 7.4) and balanced for 30min, followed by incubation in KRBB containing 2.8mmol/l (basal concentration) or 16.7mmol/l (stimulatory concentration) glucose for 1h at 37°C. Insulin released into the supernatant and the insulin content of the cells after acid/ethanol extraction (75% ethanol containing 1.5% (v/v) HCl) was measured using ELISA kits (Millipore).

The insulin secretion was normalized to protein content. Size-matched islets were placed in glass tubes containing HEPES Krebs solution containing 0.5% BSA supplemented with glucose 5mM. Islets were centrifuge for 5min after adding acid ethanol for the insulin measurements described above.

Western blot

For plasma membrane (PM) protein, isolation was used Minute™ Plasma Membrane Protein Isolation Kit (Invent Biochnologies). Approximately 20 μg sample proteins were loaded into 10% Mini-RROTEAN TGX SDS-Stain -Free Precast gels (Bio-Rad) and subjected to electrophoresis. The separated proteins were transferred to polyvinylidene fluoride membranes (Millipore) at 250 mA per gel for 2.5 h. After transfer, the membrane was blocked with blocking buffer and was incubated with a blocking buffer for 1.5h at room temperature, followed by overnight incubation with 1:1000 dilution of the KCNH6 antibody (Sigma) at 4°C. Other antibodies were listed as follows: CHOP antibody (1:1000, Cell signaling Technology); GRP78 antibody (1:1000, Abcam); caspase 3 (1:500, Cell signaling Technology) and β-actin (1:1000, Cell signaling Technology). After being washed with TBST for three times, the blots were incubated for 1h with horseradish peroxidase (HRP)-labeled donkey-anti Rabbit IgG (1:2000, Santa Cruz Biotechnology). After washing, the blots were detected by ECL chemiluminescence (Bio-Rad).

β-Cell Mass Quantification

The method was described as before (Brouwers et al., 2014). The total surface area of insulin-positive cells (in pixels) was quantified with Zeiss Axiovision of aware. The relative insulin surface area per section (total insulin area [pixels]/total pancreas area [pixels]) was multiplied by the pancreas weight (mg) to obtain the β cell mass (mg).

Total pancreas insulin content

For determination of whole-pancreas insulin content, pancreas was immediately removed and placed in 4 mL of ice-cold acid ethanol. After being weighed, the samples were manually minced and allowed to extract at −20°C for a minimum of 18h. After neutralization with 10N NaOH, cellular debris was removed by centrifugation for 5 min at 1,000 g at 4°C. The supernatant was removed and diluted 1:10,000 for the insulin measurements described above. Total pancreas insulin content was calculated as pancreas weight (μg) divided by the insulin level (μU/ml).

Intracellular Calcium Level Measurement

The $[Ca^{2+}]i$ in INS-1 β-cells or pancreatic β-cells were determined using Ca^{2+}-sensitive fluorescent indicator dye Calcium Orange (Thermo). Cells were loaded with 5 μmol/l Calcium Orange dissolved in HANKS buffer containing 0.005% Pluronic F-127 (Thermo) at 37°C in the dark for 20min. Cells were transferred in the KRBB buffer with 2.8mmol/l glucose for 5min at 37°C. Fluorescence measurements were carried out using an argon ion laser (excitation: 561 nm) using a Leica TCS SP confocal laser. Images were recorded every 15 s for 5min. Baseline fluorescence (F0) was determined by averaging 20 images. Then cells were transferred in the KRBB buffer with 16.7mmol/l glucose, images were recorded every 15 s for 15min. Fractional fluorescence (F/F0) indicates the changes of intracellular calcium concentration. Image acquisitioned analysis was with an Ultra VIEW Vox confocal imaging system (PerkinElmer).

QUANTIFICATION AND STATISTICAL ANALYSIS

Data analysis

All statistical analyses were conducted with the software MedCalc version 11.4 or GraphPad Prism version 7. Data are presented as mean ± SEM, and statistical Statistical details for individual experiments can be found in the figure legends.

Experiments performed in *Kcnh6* KO mice (Figure 4) and *Kcnh6* p.P235L KI mice (Figure 5) regarding the most important data, glucose stimulated insulin secretion (GSIS) and intraperitoneal Glucose tolerance test (IPGTT) were carried out at least three times with consistent results and one representative of each experiment is shown. *$p < 0.05$, **$p < 0.01$, ***$p < 0.001$.

DATA AND SOFTWARE AVAILABILITY

Data Resources

The accession numbers for the data of next generation sequencing on four affected individuals form the diabetes pedigree and Sanger sequencing verification of KCNH6 gene Mut in the whole family and in a panel of 99 patients with multigenerational diabetes reported in this paper are SRA: PRJNA506803.